Applied Thermal Engineering 245 (2024) 122878

Contents lists available at ScienceDirect

Applied Thermal Engineering

journal homepage: www.elsevier.com/locate/ate

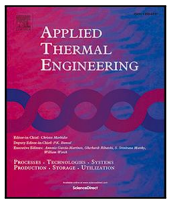

Research Paper

Analytical modelling and optimisation of a solar-driven cooling system enhanced with a photovoltaic evaporative chimney

J. Ruiz *, P. Martínez, F. Aguilar, M. Lucas

Instituto de Investigación en Ingeniería de Elche, Universidad Miguel Hernández, Avda. de la Universidad, s/n, 03202 Elche, Spain

ARTICLE INFO

Keywords:
Solar cooling
Solar chimney
Evaporative cooling
HVAC

ABSTRACT

Solar-driven heat pump systems can significantly reduce the energy use in buildings, thereby contributing to meet Europe's climate commitments, including building decarbonisation by 2050. The research gap filled by this study is the development of an analytical model of a novel photovoltaic evaporative cooling chimney system previously described in the literature. The models for the system components were validated with experimental data, showing a maximum difference of 5.83%.

An optimisation analysis based on the grid energy efficiency ratio as key performance indicator was conducted. The condenser water flow rate was identified as the key variable in this analysis. For a given design environmental and operating conditions, the optimal value for this magnitude was 1.05 $m^3\ h^{-1}$, enabling a 3.8 kW load with only 44.33 W from the grid.

The ambient temperature and relative humidity have the greatest influence on the overall system performance. They affect both, the panels' efficiency and the chiller performance. Their combined influence could lead to a 10.86% reduction in the energy use while meeting the cooling load.

The comparative study considering other solar cooling systems, assessed that the use of the solar chimney and the water–water heat pump enhances the overall performance of the main components of the system: 53% improvement for the chiller and 10% for the PV panels. Both effects combined, lead to an average grid energy efficiency ratio of 11.58.

This study provides valuable insights for the design and implementation of efficient solar-driven cooling technologies, advancing beyond previous efforts in the literature.

1. Introduction

Solar cooling refers to the use of solar energy to provide cooling for buildings or processes. It is an environmentally friendly and energy-efficient approach to cooling that can help reduce the carbon footprint associated with traditional cooling systems, thereby contributing to meet Europe's climate commitments, including building decarbonisation by 2050. The conversion of solar energy into refrigeration is achieved either through photovoltaic (PV) panels, usually referred to as PV solar cooling, or solar thermal collectors, termed as solar thermal cooling. PV cooling systems use solar PV panels to generate electricity, which is used to drive, totally or partially, the compressor of an air conditioning system (heat pumps). The supplied renewable energy equals the energy savings from the grid, resulting in a direct reduction of CO_2 emissions and non-renewable primary energy consumption. Solar thermal cooling systems use solar collectors to capture and convert solar energy into thermal energy (heat). This heat can then be used in absorption chillers or desiccant cooling systems to provide cooling. While solar thermal cooling is well-suited for applications that require a high cooling load and where the integration of solar collectors is feasible, PV cooling is versatile, relatively easy to install, can be integrated into existing structures, and can be used in a wide range of applications, including residential, commercial, and industrial buildings. Several studies can be found in the literature comparing solar thermal and PV cooling systems. According to Mugnier et al. [1], PV cooling systems are the most promising and close to market solar solution today in the case of small to medium units (≤ 50 kW $_{th}$). Neyer et al. [2] compared the performance and economic feasibility of solar thermal and PV cooling systems in two different buildings, a hotel in Austria and a small multifamily house in Madrid. The authors concluded that thermal systems achieved higher efficiency and savings in applications with a higher thermal demand whereas PV cooling systems are more suitable for residential or small-scale tertiary applications, where the thermal demand is lower. Similar conclusions were reached by Hakemzadeh et al. [3]. In this study, the authors estimated the

* Corresponding author.
E-mail address: j.ruiz@umh.es (J. Ruiz).

https://doi.org/10.1016/j.applthermaleng.2024.122878
Received 21 November 2023; Received in revised form 5 February 2024; Accepted 4 March 2024
Available online 6 March 2024

Nomenclature

A	PV collector area (m^2)
$a-f$	constants in Eqs. (20) and (21) (-)
a_V	surface area of exchange per unit of volume (m^2 m^{-3})
c_p	specific heat (J kg^{-1} K^{-1})
EER	energy efficiency ratio (-)
$\overline{G}$	solar insolation (Wh m^{-2})
G	solar irradiance (W m^{-2})
g	gravitational acceleration (m s^{-2})
h	enthalpy (J kg^{-1})
h_C	heat transfer coefficient (W m^{-2} K^{-1})
h_D	mass transfer coefficient (kg m^{-2} s^{-1})
h_e	external heat transfer coefficient (W m^{-2} K^{-1})
h_i	internal heat transfer coefficient (W m^{-2} K^{-1})
H_m	manometric head (m)
k	thermal conductivity (W m^{-1} K^{-1})
k_r	rotational speed ratio (-)
Le	Lewis number ($= h_C / \left(h_D c_{p_{ma}}\right)$)
$\dot{m}$	mass flow rate (kg s^{-1})
Me	Merkel number ($= h_D a_V V / \dot{m}_w$)
Q	volumetric flow rate (m^3 s^{-1})
$\dot{Q}$	heat rate (W)
T	temperature (°C)
V	volume of the transfer region (m^3)
v_i	velocity in the convective area (m s^{-1})
v_w	wind velocity (m s^{-1})
W	work (J)
$\dot{W}$	power (W)
x	thickness (m)
z	height (m)

Greek symbols

β	temperature correction factor (°C^{-1})
η	efficiency (-)
γ	irradiance correction factor (-)
Ω	rotational speed of the pump (s^{-1})
ω	humidity ratio (kg kg^{-1})
ρ	density (kg m^{-3})
τ	reflectivity (-)

Subscripts

a	air
c	cell
comp	compressor
cond	condenser
e	electric
evap	evaporator
g	glass
grid	grid
i	intermediate
pump	pump
r	rear
ref	reference conditions
ref,NOCT	reference conditions for NOCT calculation
s_w	saturated at T_w
t	tedlar
th	thermal
v	vapour
w	water
1	inlet
2	outlet

Abbreviations

CFD	Computational Fluid Dynamics
EER	Energy Efficiency Ratio
NOCT	Nominal Operating Cell Temperature
PV	Photovoltaic
VFD	Variable Frequency Drive

techno-economic potential and environmental compatibility of solar absorption and adsorption cooling systems for a tropical climate. They concluded that the initial investment and the cost of the equipment must be reduced to achieve a competitive advantage compared to other cooling systems in low-demand applications.

It has been extensively reported in the literature that PV cooling can reduce significantly the primary energy consumption in buildings by improving the efficiency of conventional HVAC systems. Table 1 summarises some of the most relevant studies addressing this topic. One way to improve the efficiency of PV systems involves increasing the conversion efficiency of solar energy into electricity. The performance of conventional PV cells depends on three physical parameters: the intensity of the solar radiation flux, the quality of the semiconductor in use, and the operating temperature of the cell. In a traditional PV panel, typically 10%–20% of the radiated solar energy is converted into electricity while the remainder is transformed into heat. This fact causes heating of the solar cells in PV panels resulting in a drop in the conversion rate of about 0.5%/°C, [4]. In summer periods where the panel can experience temperatures ranging 40–70 °C, the drop of maximum power production can be up to 7.5%–22%. Because of this fact, the temperature regulation of photovoltaic panels is of paramount importance.

Some authors have presented comprehensive reviews of the common methods utilised for cooling PV panels, [13,14]. The different PV cooling approaches can be classified into active and passive techniques. Active methods include air cooling [15–17], liquid cooling [18,19] and liquid spray [20,21]. In all the papers reviewed, authors reported significant benefits regarding the PV panel performance. The efficiency of the active cooling methods is primarily affected by the geometry of the cooling channels as well as their mass flow rates and the type of coolant used. Passive techniques encompass heat pipes, Phase Changing Materials (PCM) and wick structure. Heat pipes represent a two-phase thermal transfer device that harnesses the latent enthalpy associated with phase changes, and they find extensive application across diverse systems designed for efficient cooling of high heat fluxes such as in PV applications, [22,23]. PCMs absorb the excess thermal energy of the cell as latent heat of fusion, in constant temperature in which phase transition occurs. The work of Chandel et al. [24] presents a complete review of studies combining PV and PMC.

Every applied approach for the thermal management of PV panels carries with it a distinct set of advantages and disadvantages. The main advantage associated with active methods lies in their higher heat removal capacity, at the expense of the external source of energy consumption to create the fluid flow and the more intricate structure required for supplementary equipment. On the other hand, passive approaches offer significant advantages in the form of their straightforward design (simpler structure), absence of additional devices and

Table 1
Literature review addressing the use of PV cooling systems used in cooling applications.

Reference	Methodology	Main results
Ji et al. [5]	Experimental and simulation	Study of a photovoltaic solar assisted heat pump (PV-SAHP) with PV-Thermal collector. Experimental and simulation maximum COP of the PV-SAHP of 8.4 with an average PV efficiency of 13.4%.
Fong et al. [6]	Simulation	Five types of solar cooling systems were, including: electric compression, mechanical compression, solar absorption, adsorption and solid desiccant. Solar electric compression with PV panels had one of the highest energy saving potential in the study.
Otanicar et al. [7]	Modelling	Economic and environmental analysis of a variety of solar cooling systems (thermal and PV assisted heat pumps). PV cooling presented a lower projected emission value of carbon dioxide per kWh_{th} of cooling than any of the studied thermal technologies.
Al-Alili et al. [8]	Review	Review of several solar cooling technologies, including thermal and electrical systems.
Ghafoor and Munir [9]	Review	The overall efficiency of solar thermal cooling technology is still lower than that of the vapour compression cycles.
Aguilar et al. [10]	Experimental	Experimental study conducted in an air-conditioning system powered by a PV facility and the grid simultaneously. Results obtained for 6 months of operation in cooling mode demonstrated that the average COP of the proposed system was close to 15, with a solar contribution near 65%.
Song et al. [11]	Modelling	Three hybrid heat pump systems based on different solar concentrators are designed and investigated in this paper. The high temperature problem is alleviated by combining concentrated PV with a direct expansion heat pump (higher electrical and exergy efficiencies).
Sulaiman et al. [12]	Modelling	A solar-powered air-conditioning bed unit is investigated in this paper. Propane is a potential alternative for R134a as a natural refrigerant.

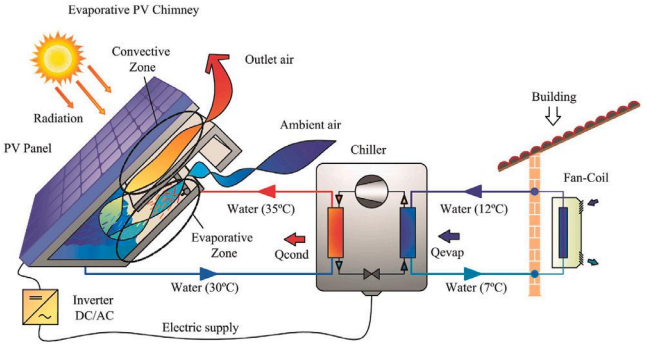

Fig. 1. Diagram illustrating the layout and operation of the PV evaporative chimney system.

equipment, as well as their generally lower maintenance costs in comparison to active methods. This cost efficiency is mainly attributed to the lower number of equipment and media used in passive approaches. Passive techniques should be used in highly-ventilated areas, respecting the distance between panels and between the panels and the architectural elements of the surroundings, such as facade walls. It is advisable to avoid configurations involving architectural integration since, although they reduce visual impact, they hinder proper panel ventilation. This leads to an increase in the working temperature of the panels, significantly reducing their efficiency.

The photovoltaic evaporative solar chimney is a system whose primary purpose is to enhance the efficiency of solar photovoltaic modules through evaporative cooling. The system has been previously described in the literature and a schematic representation of its components and operation is depicted in Fig. 1. It comprises a solar chimney attached to the rear of the PV panel, increasing panel performance by cooling it via the buoyancy-driven airflow induced within the chimney. Additionally, in the designated evaporative area, a series of nozzles spray water parallel to the downward airflow. As the water descends, a portion evaporates, cooling the remaining water. This area operates like a small-scale cooling tower. The air that has come into contact with the water may experience a temperature reduction (depending on ambient conditions), thereby enhancing the cooling effect on the panel. Since the water used for cooling the modules can also be utilised for the condensation of a refrigeration cycle, the system also enhances the efficiency of the heat pump, constituting a water-cooled system (no need of a cooling tower). Consequently, the advantages of the photovoltaic evaporative chimney are twofold.

The system was initially described by Lucas et al. [25]. The authors documented the operation of two PV collectors, with one serving as a reference and the other modified on its rear to include the evaporative solar chimney. The system had the capacity to dissipate thermal power of approximately 1.5 kW, achieving a thermal efficiency exceeding 30% in summer conditions. Temperature differences between the cooled module and the reference module reached up to 8 °C, depending on wind conditions and ambient air properties. This resulted in an enhancement of electrical efficiency of up to about 8% in comparison to nominal efficiencies. Subsequently, in Lucas et al. [26], the authors explored the modification of the evaporative photovoltaic chimney's performance through the addition of a water slide system on the upper surface of the photovoltaic panel. This adjustment aimed to address certain operational challenges observed in the initial prototype, such as non-uniform temperature distribution across the module and the adverse effects of high-wind conditions on system operation. The outcomes revealed an average cooling effect of 15 °C on the panel and a 10% improvement in the electrical efficiency of the panel. The modified system retained the capacity to dissipate thermal power of around 1.5 kW, maintaining a thermal efficiency exceeding 30% during summer conditions. However, these studies were limited to evaluating the performance of the panel and the evaporative chimney, without assessing the system's operation when connected to a water-cooled chiller for heat dissipation from a building. More recently, in Ruiz et al. [27], the same group of researchers undertook a systematic study where the performance of a system comprising 4 PV panels with their evaporative chimneys operated alongside a water–water chiller. Through an experimental analysis in a Mediterranean climate, the authors reported an average conversion of solar energy into refrigeration capacity of 0.49. The system achieved a 64.40% solar contribution and delivered an average of 11.32 kWh of cooling per each electric kWh consumed from the grid, exhibiting its potential for energy-efficient cooling in the building sector. In another study conducted by Casado et al. [28], the authors dealt with the design and implementation of an I–V curve measurement system to be used in the performance analysis of the system.

The motivation for undertaking this work was justified by the limitations found in the aforementioned studies, primarily associated with the employed methodology. The experimental approach does not allow for the control of certain variables that have a significant impact on the operation of the equipment (environmental conditions) or the independent analysis of some of those variables (for example, ambient humidity and temperature are often linked, depending on the location where the system is operating). Hence, the obtained data cannot be extrapolated to other geographical locations, used to optimise the operation of the system, or guide decision-making on the design for a specific application. Thus, the research gap filled by this paper is the development of an analytical model of the PV evaporative cooling chimney system described in [27], validated with experimental data.

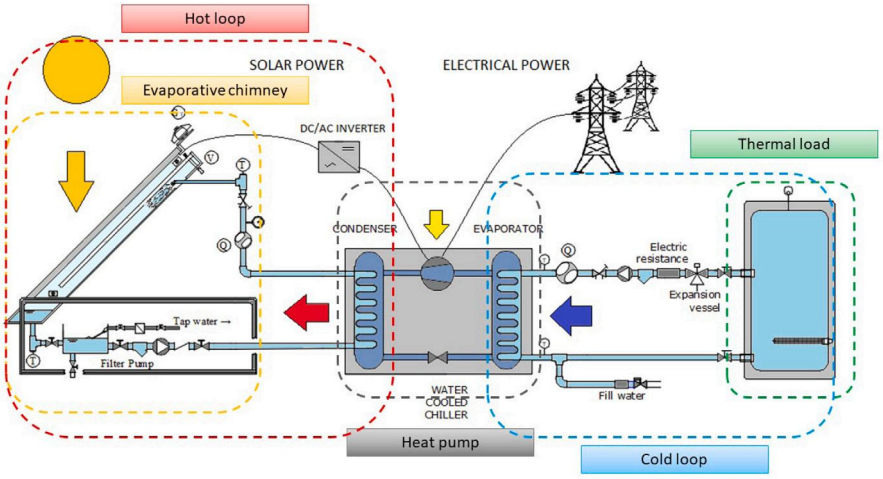

Fig. 2. Schematic arrangement of the PV evaporative chimney system.

The system consists of 4 PV evaporative chimneys (4×255 W_p) and a 3.8 kW water–water heat pump. The model is employed in this research to analyse the impact of certain environmental variables on the system's performance independently, optimise the operation to achieve the best energy performance under given environmental and operating conditions, and compare its energy performance with that of other systems reported in the literature.

This paper is organised as follows: Section 2 details the models used in the analysis and how the are connected. Next, the validation of the models, an optimisation analysis, a parametric study concerning the ambient conditions, and a comparative analysis with another solar cooling system are presented and discussed in Section 3. Finally, the most important findings of the research are summarised in Section 4.

2. Mathematical modelling

The PV evaporative solar chimney integrated in an air-conditioning scheme (water–water chiller) is shown in Fig. 2. As it can be observed, it consists of 5 subsystems: PV evaporative chimney, heat pump, hot and cold water loops and thermal (cooling) load. The *cooling load* constitutes the first subsystem and represents the thermal energy gain of the system, encompassing factors such as lighting, occupancy, structural elements, and radiation. Under normal circumstances, these gains must be dissipated to the environment by the HVAC system. The heat rate gained due to the load is transferred to the heat pump by means of the *cold loop*. It consists of a network of pipes and a hydraulic pump that circulates the heat carrier fluid. The *water-cooled heat pump* subsystem pumps the cooling thermal load and the heat generated by the compressor into the hot water circuit. Here is where the heat exchange between the thermal loops takes place. The *hot loop* connects the heat pump and the evaporative chimney. As in the cold loop, a piping system (pipes and pump) is used to transport the heat carrier fluid (water) between subsystems. Finally, at the *PV evaporative chimney subsystem*, the heat is delivered to the atmosphere by means of evaporative heat transfer process. Moreover, the airflow induced because the buoyant force due to the solar collectors heating, cool the panels and increase the power generated by the system. This electricity is used to drive (totally or partially) the compressor of the heat pump and the pump of the hot loop.

A global mathematical model was developed to predict the performance of the system. It includes three of the five subsystems previously described: water–water chiller, condenser (hot) loop and photovoltaic evaporative chimney. The cooling load and the cold circuit are strongly related to the specific application. Accordingly, their models were not included in the global model.

The cooling load was taken constant and equal to 3.8 kW, matching the nominal conditions of the mechanical chiller. This fact was justified due to the fact that the cooling load depends on several factors, such as building geometry, construction materials or location. Besides, in the experimental setup of [27] a 3.8-kW-water heater was used to simulate the cooling load. Concerning the cold loop, it was considered that the energy consumed by the pump would the same regardless of the type of air conditioning system used. Therefore, this system was modelled taking into account an evaporator inlet water temperature of 7 °C, as in typical air conditioning applications. As the condenser water loop is present in this specific application, the energy consumption of this pump must be included in the analysis since it contributes significantly to the overall operating cost.

2.1. Photovoltaic evaporative chimney

The performance of the photovoltaic evaporative chimney can be studied by dividing the system into two different areas: the convective and evaporative areas. The link between these two different zones is the temperature of the air leaving the evaporative area (which matches the air temperature entering the convective area). The solar collectors convert the heat rate emitted by the sun into electric power. A portion of this heat rate is absorbed, another portion is reflected and the remainder is transmitted to the collector cells. A part of the transmitted heat rate is converted into electricity and the remainder is transformed into heat, which is dissipated in the front and rear sides of the panel by means of convection. The heat not evacuated causes heating of the solar cells in PV panels resulting in a drop in the conversion rate.

2.1.1. Convective area

A 1D model was considered in this paper for the convective area, and it takes into account the steady-state energy balance for each element in the solar plate, Eqs. (1)–(4). It was considered that the PV panel is formed by PV cells protected by a glass on the front and a plastic material (tedlar) on the rear. In the undertaken analysis, it was assumed that the glass reflects a portion of the incoming radiation. The Fresnel and Snell laws were used to the determine the reflectivity (τ) as a function of the month, day and hour of the year. The results showed a fairly constant value for the reflectivity throughout the year, ranging from 0.85–0.9. Accordingly, a constant value of $\tau = 0.9$ was considered in the analysis. It was also assumed that all the heat rate passing through the glass was absorbed by the cell (silicon).

$$h_e A \left(T_g - T_{\text{amb}}\right) = \frac{A k_g}{x_g} \left(T_c - T_g\right) \tag{1}$$

$$GA\tau = \eta_{PV} GA + \frac{Ak_g}{x_g}\left(T_c - T_g\right) + \frac{Ak_c}{x_c}\left(T_c - T_t\right) \quad (2)$$

$$\frac{Ak_c}{x_c}\left(T_c - T_t\right) = \frac{Ak_t}{x_t}\left(T_t - T_r\right) \quad (3)$$

$$h_i A\left(T_r - T_i\right) = \frac{Ak_t}{x_t}\left(T_t - T_r\right) \quad (4)$$

The heat dissipated from the front a rear sides of the panel was calculated using the convection coefficients (h_e, h_i) reported by Aguilar [29], Eqs. (5)–(6). They depend linearly on the wind and convection area velocities, respectively.

$$h_e = 0.841 v_w + 4.61 \quad (5)$$

$$h_i = 1.97 v_i + 10 \quad (6)$$

where the velocity in the convective area, v_i, was obtained using the experimental relationship reported by [25]. The velocity in this area depends on the buoyancy-driven flow induced due to the heating of the air by the panels and the momentum transfer between sprayed water and air. As stated by the authors, the predominant mechanism is due forced convection rather than natural convection. Therefore, v_i can be expressed as a function of the mass flow rate of sprayed water ($\dot{m}_w$), Eq. (7).

$$v_i = -207.325\dot{m}_w^2 + 67.978\dot{m}_w - 2.380 \quad (7)$$

The system of algebraic equations is closed by including the electrical efficiency of the panel-cell temperature relationship. Skoplaki and Palyvos [30] conducted a comprehensive literature review and proposed several correlations to determine the PV efficiency (η_{PV}) as a function of its temperature. Three different correlations were considered in this analysis, Eqs. (8)–(10).

$$\eta_{PV} = \eta_{PV,ref}\left(1 - \beta_{ref}\left(T_c - T_{ref}\right)\right) \quad (8)$$

$$\eta_{PV} = \eta_{PV,ref}\left[1 - \beta_{ref}\left(T_c - T_{ref}\right) + \gamma \log_{10}\left(\frac{G}{G_{ref}}\right)\right] \quad (9)$$

$$\eta_{PV} = \eta_{PV,ref}\left[1 - \beta_{ref}\left(T_{amb} - T_{ref} + \left(T_{NOCT} - T_{ref,NOCT}\right)\frac{G}{G_{ref,NOCT}}\right)\right] \quad (10)$$

Eq. (8) represents the traditional linear expression for the PV electrical efficiency. Here, $\eta_{PV,ref}$ is the module's electrical efficiency at the reference temperature, T_{ref} = 25 °C, and at solar radiation flux of G_{ref} = 1000 W m^{-2}, and β_{ref} is the temperature correction factor. These quantities are normally provided by the PV manufacturer ($\eta_{PV,ref}$ = 0.157 and β = 0.0044 °C^{-1} for the PV panels considered in this research). The γ constant in Eq. (9) was determined by fitting the equation to the experimental data provided by [27]. The obtained value was γ = 0.02748. Eq. (10) is used when the module/cell temperature is not readily available. T_{NOCT} is the module temperature at the ambient temperature of $T_{ref,NOCT}$ = 20 °C and the solar irradiance of $G_{ref,NOCT}$ = 800 W m^{-2}, Eq. (11), [31,32]. The value is approximately 45 ± 2°C for monocrystalline and polycrystalline PV modules, [33]. Generally, the NOCT is constant for PV module and the value is given by manufacturer (T_{NOCT} = 47 °C). It can be easily derived that Eq. (10) is obtained by substituting the Eq. (11) into Eq. (9).

$$T_c = T_{amb} + \left(T_{NOCT} - T_{ref,NOCT}\right)\frac{G}{G_{ref,NOCT}} \quad (11)$$

The electrical power generated by the panels is determined via the collector efficiency, the collector area (A) and the global irradiance (G), Eq. (12).

$$\eta_{PV} = \frac{\dot{W}_{PV}}{GA} \quad (12)$$

By solving this set of algebraic equations (1)–(4) alongside the efficiency of the collector, Eqs. (8), (9) or (10), the temperature distribution along the panel is determined, including T_c and T_i. They are used to calculate the panel electrical performance and to link the convective and evaporative areas, respectively.

2.1.2. Evaporative area

In the evaporative area, heat and mass between water and air are transferred. Water flows downwards from the nozzles to the tower basin (where is finally collected) in parallel to the air stream (parallel flow arrangement). As stated in Section 1, this area works as a small-scale cooling tower. The Merkel number is the accepted dimensionless coefficient of performance of a wet cooling tower, [34]. This dimensionless number is defined in Eq. (13), and it measures the degree of difficulty of the mass transfer processes occurring in the exchange area of a cooling tower.

$$\mathrm{Me} = \frac{h_D a_v V}{\dot{m}_w} \quad (13)$$

The computation of the Merkel number can be done using two established theories for evaluating cooling tower performance: the Merkel and Poppe theories. The Merkel theory [35], while historically significant, relies on several critical assumptions, including the assumption that the Lewis factor equals 1, that the air exiting the tower is saturated with water vapour, and that the reduction in water flow rate due to evaporation is disregarded in the energy balance. Consequently, the Poppe theory [36] is generally favoured for its more comprehensive approach. Within the Poppe theory, the authors derived governing equations for heat and mass transfer in the transfer region of the cooling tower. According to the Poppe theory, the major following equations for the heat and mass transfer are obtained:

$$\frac{d\omega}{dT_w} = \frac{c_{p_w}\frac{\dot{m}_w}{\dot{m}_a}\left(\omega_{s_w} - \omega\right)}{\left(h_{s_w} - h\right) + (\mathrm{Le} - 1)\left[\left(h_{s_w} - h\right) - \left(\omega_{s_w} - \omega\right)h_v\right] - \left(\omega_{s_w} - \omega\right)h_w} \quad (14)$$

$$\frac{dh}{dT_w} = c_{p_w}\frac{\dot{m}_w}{\dot{m}_a} \times \left[1 + \frac{\left(\omega_{s_w} - \omega\right)c_{p_w}T_w}{\left(h_{s_w} - h\right) + (\mathrm{Le} - 1)\left[\left(h_{s_w} - h\right) - \left(\omega_{s_w} - \omega\right)h_v\right] - \left(\omega_{s_w} - \omega\right)h_w}\right] \quad (15)$$

$$\frac{d\,\mathrm{Me}}{dT_w} = \frac{c_{p_w}}{\left(h_{s_w} - h\right) + (\mathrm{Le} - 1)\left[\left(h_{s_w} - h\right) - \left(\omega_{s_w} - \omega\right)h_v\right] - \left(\omega_{s_w} - \omega\right)h_w} \quad (16)$$

The detailed derivation process and simplification of the governing equations of the Poppe theory, as well as the solving procedure using the fourth order Runge–Kutta method, can be found in [34,37]. Due to the water and air flows arrangement, the Poppe theory was adapted for parallel flow arrangement, which is much less common than the counterflow variant (standard one). The difference between variants lies in the boundary conditions used (the set of equations remains the same). When the set of Eqs. (14)–(16) is solved, the evolution of the air humidity, the air enthalpy, the water temperature, the water mass flow rate and the Me in the transfer region of the cooling tower are obtained.

In wet cooling towers, the Merkel number corresponding to different operating conditions can be correlated in terms of the water-to-air mass flow ratio. In the case of the evaporative area of the prototype, the experimental relationship determined by [25] for Me is defined in Eq. (17):

$$\mathrm{Me} = 0.7099\left(\frac{\dot{m}_w}{\dot{m}_a}\right)^{-0.3254} \quad (17)$$

The air mass flow rate, $\dot{m}_a$, and, consequently, the water-to-air mass flow ratio were experimentally found to be proportional to the water mass flow rate, $\dot{m}_w$. This was justified due to the momentum transfer between water and air. The experimental relationship for the water and air mass flow rates found in [25] is shown in Eq. (18).

$$\dot{m}_a = -6.1751\dot{m}_w^2 + 2.2469\dot{m}_w - 0.07653 \quad (18)$$

2.2. Water-cooled chiller

The performance of a refrigeration cycle is usually described by the Energy Efficiency Ratio (EER), Eq. (19), which measures the ratio of

Table 2
Fitting coefficients for Eqs. (20)–(21).

Equation/coefficient	*a*	*b*	*c*	*d*	*e*	*f*
Eq. (20)	12.15	−1.826	0.2108	0.1166	0.004213	−0.05686
Eq. (21)	6.331	0.2215	0.1163	–	–	–

cooling power to electrical power.

$$\mathrm{EER} = \frac{\dot{Q}_{\mathrm{evap}}}{\dot{W}_{\mathrm{comp}}} = \frac{\dot{Q}_{\mathrm{cond}} - \dot{W}_{\mathrm{comp}}}{\dot{W}_{\mathrm{comp}}} = \frac{\dot{Q}_{\mathrm{evap}}}{\dot{Q}_{\mathrm{cond}} - \dot{Q}_{\mathrm{evap}}} \tag{19}$$

The EER depends mainly on condensation and evaporation temperatures, T_{cond} and T_{evap}. As suggested by several scientific and technical Refs. [38–41], the behaviour of the chiller as a function of the above-mentioned temperatures can be described by linear and quadratic relationships. The condenser inlet water temperature ($T_{w_{1_{\mathrm{cond}}}}$) and the evaporator outlet water temperature ($T_{w_{2_{\mathrm{evap}}}}$) were used instead in the present work for convenience. The pair of temperatures $T_{w_{1_{\mathrm{cond}}}} - T_{\mathrm{cond}}$ and $T_{w_{2_{\mathrm{evap}}}} - T_{\mathrm{evap}}$ are linked via the heat exchange thermal approach. Accordingly, the two correlations considered in this analysis are shown in Eqs. (20)–(21).

$$\mathrm{EER} = a + bT_{w_{2_{\mathrm{evap}}}} + cT_{w_{2_{\mathrm{evap}}}}^2 + dT_{w_{1_{\mathrm{cond}}}} + eT_{w_{1_{\mathrm{cond}}}}^2 + fT_{w_{2_{\mathrm{evap}}}}T_{w_{1_{\mathrm{cond}}}} \tag{20}$$

$$\mathrm{EER} = a + bT_{w_{2_{\mathrm{evap}}}} + cT_{w_{1_{\mathrm{cond}}}} \tag{21}$$

The coefficients shown in Table 2 were obtained by fitting the experimental data reported in [27].

It should be noted that the condenser inlet and outlet water temperature ($T_{w_{1_{\mathrm{cond}}}}$, $T_{w_{2_{\mathrm{cond}}}}$) match the evaporative area outlet and inlet water temperatures (T_{w_2}, T_{w_1}), respectively.

2.3. Condenser (hot) loop

The condenser or hot loop can be characterised by the volumetric flow rate and the pressure head in the piping network. As in most engineering flows (fully developed, turbulent pipe flow), head losses are roughly proportional to the square of the flow rate. This relationship can be obtained by applying a mechanical energy balance between liquid levels at the suction and discharge points, obtaining the well-known relationship $H_m = H_g + CQ^2$. Here, H_m is the pumping head, H_g is the static head difference, Q is the rate of flow and C is a constant that includes friction and minor losses in the pipes as well as the losses due to the spray nozzles. The performance curve of the condenser loop is shown in Eq. (22) (H_m in m and Q in l s^{-1}), which was obtained by means of EPANET software.

$$H_m = 1 + 89.649Q^2 \tag{22}$$

The pumping energy consumption, $\dot{W}_{\mathrm{pump}}$, is proportional to the pumping head, the water flow rate, and pump efficiency, η_{pump}, Eq. (23).

$$\eta_{\mathrm{pump}} = \frac{\rho_w g Q H_m}{\dot{W}_{\mathrm{pump}}} \tag{23}$$

The data provided by the pump manufacturer for the nominal operating frequency was used to fit the coefficients in Eqs. (24)–(25), which are typical expressions to represent the $H_m - Q$ and $\eta_{\mathrm{pump}} - Q$ relationships. The obtained values were $H_0 = 45.05$ m, $Q_0 = 1.308$ l s^{-1}, and $\eta_{\mathrm{pump}_0} = 3.4$.

$$H_m = H_0\left[1 - \left(\frac{Q}{Q_0}\right)^2\right] \tag{24}$$

$$\eta_{\mathrm{pump}} = \eta_{\mathrm{pump}_0}\left(\frac{Q}{Q_0}\right)\left(1 - \frac{Q}{Q_0}\right) \tag{25}$$

In order to set the desired operation point (volumetric flowrate in the chimneys), a Variable Frequency Drive (VFD) was used to control the pump. Therefore, the efficiency equation shown in (25) should be corrected to take into account the modified rotational speed of the pump ($k_r = \Omega'/\Omega$) that satisfies the desired operating point given the volumetric flow rate and the system curve. Eqs. (26)–(27) show the pump characteristics taking into account the change of rotational speed required to meet the desired operating point. The affinity laws for centrifugal pumps were used to predict pump performance for changes in impeller speed.

$$H'_m = H_0 k_r^2\left[1 - \left(\frac{Q}{k_r Q_0}\right)^2\right] \tag{26}$$

$$\eta'_{\mathrm{pump}} = \eta_{\mathrm{pump}_0}\left(\frac{Q}{k_r Q_0}\right)\left(1 - \frac{Q}{k_r Q_0}\right) \tag{27}$$

2.4. Interaction between models

The global model requires 7 ambient and operating variables, as well as cooling requirements as inputs: ambient temperature (T_{amb}) and relative humidity (ϕ_{amb}), global irradiance (G), wind velocity (v_w), condenser water flow rate (Q), evaporator heat rate or cooling capacity ($\dot{Q}_{\mathrm{evap}}$) and the temperature of the water leaving the evaporator ($T_{w_{2_{\mathrm{evap}}}}$). The global model predicts the operating parameters of every subsystem and the global key performance indicators (i.e. PV collector efficiency and generated power, chiller EER and compressor and pump power consumption).

The set of equations presented in this section was solved using the MATLAB software f-solve function, and the calculation sequence is depicted in Fig. 3 by means of a flowchart. The chiller and the evaporative chimney models are coupled through the condenser inlet temperature ($T_{w_{1_{\mathrm{cond}}}} = T_{w_2}$). Therefore, in the first step (Step 1) the equations for the evaporative area and the heat pump are solved concurrently. The pair of values $T_{w_1} - T_{w_2}$ that simultaneously satisfy the Merkel (system formed by Eqs. (14)–(16) and Eq. (17)) and EER equations (system formed by Eq. (19) and (20) or (21)) is obtained. As a result, all the variables involved in these subsystems are calculated. The most relevant are the chiller EER, $\dot{Q}_{\mathrm{cond}}$ and $\dot{W}_{\mathrm{comp}}$. Afterwards, in Step 2, the equations that govern the convective area are solved (system formed by Eqs. (1)–(4) and Eq. (8), (9) or (10)). The link with Step 1 is the temperature of the air leaving the evaporative area (T_{a_i}). The most important variables obtained at this stage are the PV panel efficiency and the generated power (η_{PV}, $\dot{W}_{\mathrm{PV}}$). Finally, at Step 3, the equations for the hot loop (hydraulic system) are solved. There are two differences with the previous stages. The first one is that this subsystem does not require any variable from the previous calculations. It is fed only by the water volumetric flow rate (input). The second difference is that the equations for this subsystem can be solved sequentially. This model provides $\dot{W}_{\mathrm{pump}}$.

3. Results and discussion

3.1. Experimental validation

The global model presented in Section 2 was validated using two different sets of experimental results. The experimental results presented in Lucas et al. [25] were used to validate the PV collector and evaporative chimney models. In this study, the authors conducted a comprehensive investigation, recording all the magnitudes required to characterise a PV panel operating alongside with a evaporative chimney in terms of electrical and thermal performance. Consequently, the necessary variables for validating the PV collector and evaporative chimney models were available. This set of variables includes

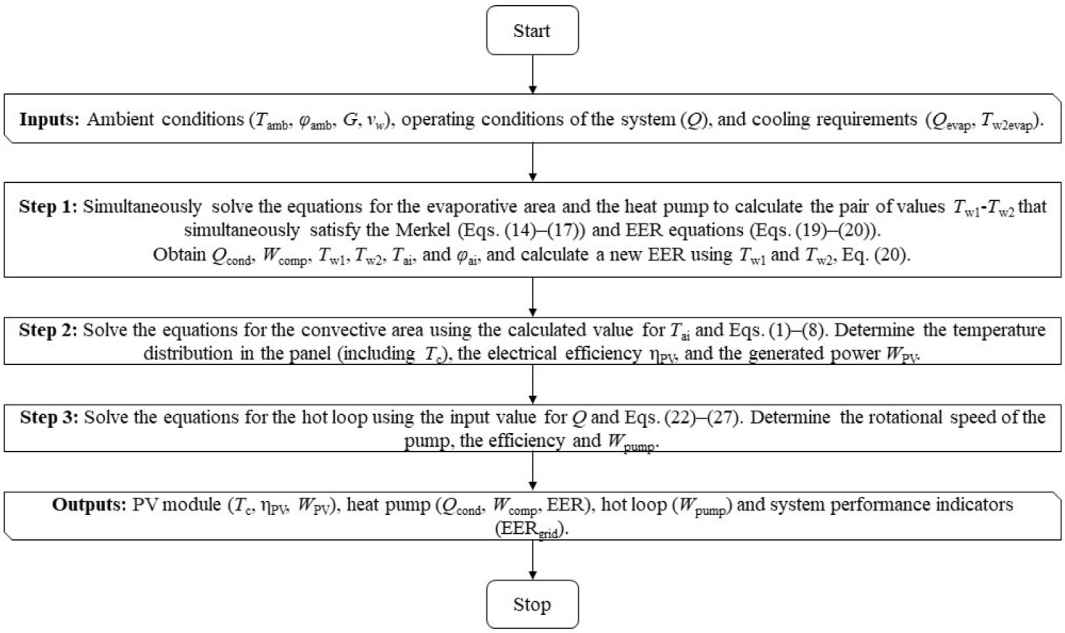

Fig. 3. Flow chart of the MATLAB code for the PV evaporative chimney system.

the PV panel temperature, efficiency and generated power, air-related variables (temperature, relative humidity, and velocity) at the inlet, intermediate, and outlet sections, as well as water-related magnitudes (temperature at the inlet and outlet sections and flow). On the other hand, the experimental results reported by Ruiz et al. [27] were employed to assess the goodness of the chiller model. In this paper, the performance of a PV solar-driven cooling system enhanced with a photovoltaic evaporative chimney was experimentally characterised. As in the model reported in this paper, the system consisted of four PV panels (1.02 kW_p nominal power) attached to their corresponding evaporative chimneys and a 3.8-kW-refrigeration-capacity water-cooled chiller. The authors reported performance values for the chiller under different ambient and operating conditions.

3.1.1. PV collector and evaporative chimney models validation

Fig. 4 shows the comparison between experimental and predicted results for the test run where $\dot{Q}_{cond}$ = 1.5 kW and Q = 375 l h^{-1} in [25]. Fig. 4(a) displays the variation of inlet and outlet water temperatures, as well as the temperature of the air leaving the evaporative area, during the test while Fig. 4(b) depicts the performance of the panel. It should be noted that the 3 correlations compared to determine the PV efficiency as a function of its temperature provided satisfactory results, but the correlation presented in Eq. (8) lead to the best results in terms of experimental-predicted difference. As it can be seen, the model successfully predicts the magnitude and variation of the operating variables of the system. For this test run, maximum differences of 0.27 and 0.38°C for inlet and outlet temperatures, respectively, were found. Regarding the electrical parameters, the difference was lower than 3.32%. The comparison between experimental and predicted results was not limited one test run, but was extended to the 3 of them, Table 3.

3.1.2. Chiller model validation

Concerning the chiller model, it was found that the results predicted by the quadratic correlation presented in Eq. (20) showed a better agreement with the experimental results from 9 tests reported by [27] than the linear correlation in Eq. (21). Although both correlations provided reasonably accurate results, the quadratic correlation lead to differences lower than 1.30% whereas the linear correlation predicted results with a difference of 2.03%. Consequently, the global model was

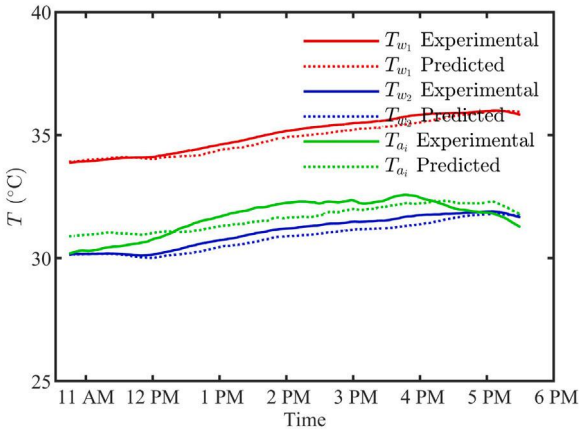

(a) Evaporative area inlet and outlet water temperatures and outlet air temperature.

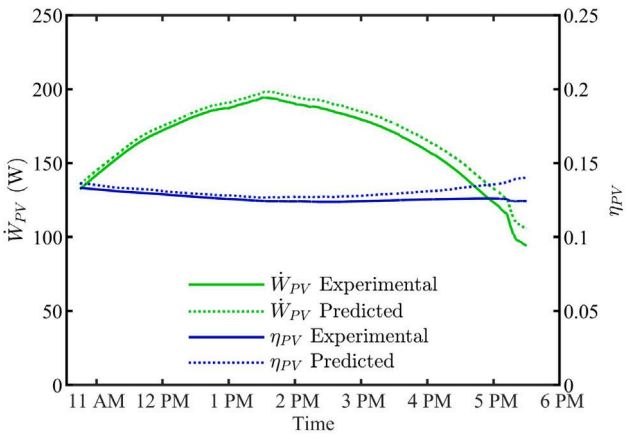

(b) Efficiency of the PV module and generated power.

Fig. 4. Comparison between experimental and predicted results for test run where $\dot{Q}_{cond}$ = 1.5 kW and Q = 375 l h^{-1} in [25].

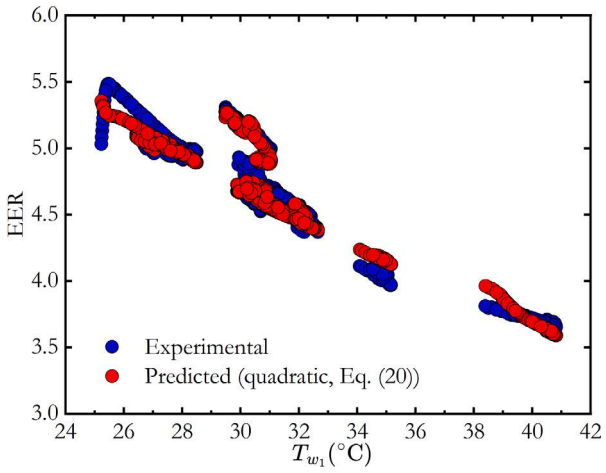

Fig. 5. Comparison between experimental [27] and predicted (Eq. (20)) results for several stationary points.

Table 3
Maximum and average difference between the experimental data reported by [25] (all the tests conducted) and the results predicted by the model.

Magnitude	Maximum difference (%)	Average difference (%)
T_{w_1}	2.221	0.8597
T_{w_2}	2.347	1.005
T_{a_i}	6.336	2.802
$\dot{W}_{PV}$	3.467	2.469
η_{PV}	5.830	2.478

considered validated. Fig. 5 shows the comparative results for different stationary points in [27] and the quadratic correlation (Eq. (20)).

3.2. Optimisation analysis

As pointed out in Section 1, one of the main advantages of having a validated model is the ability to optimise the operating conditions based on economic or energetic criteria. Consequently, this section presents an analysis aimed at finding the optimal operating conditions, based on an energetic criterion, for the proposed system consisting of four PV evaporative chimneys and a 3.8 kW nominal capacity water-cooled heat pump. The design conditions shown in Table 4 were considered. The environmental design values correspond to the hottest hour of the year in Alicante (27th of July, 12 h), southeast Spain. The chilled water temperature was set as 7 °C, as in typical air conditioning applications. The cooling load was taken equal to 3.8 kW, matching the nominal conditions of the mechanical chiller.

Taking that into consideration, it was found that the water flow rate in the condenser had the highest impact on the performance of the system. This can be explained as follows. The model for the evaporative zone of the evaporative chimney presented in Section 2 states that an increase of the water mass flow rate leads to an increase of the Merkel number. This is justified by the relationship between the water and the air mass flow rates presented in Eq. (18), which implies a higher increasing rate for $\dot{m}_a$ than for $\dot{m}_w$. Consequently, the water-to-air mass flow ratio decreases and Me increases. A higher Merkel number will result in a lower condensing temperature which favours the EER, reducing the chiller power consumption for a given cooling capacity. However, on the other hand, achieving a higher flow rate of water requires a higher pumping head, increasing the pump power consumption. Therefore, the dependence between the water flow rate and the global performance of the system is not straightforward. Those opposed effects may lead to an optimal operating point regarding power consumption.

The investigated range for Q was 250–500 l h^{-1} for each chimney (1–2 m^3 h^{-1}). This is justified because this range was used in the experiments that led to the correlations reported in Section 2.

The energetic key performance indicator used in the optimisation analysis was the grid energy efficiency ratio, EER_{grid} in Eq. (28). It relates the power supply from the grid ($\dot{W}_{grid}$) required to meet the cooling demand. $\dot{W}_{grid}$ accounts for the difference between the total consumption (compressor and pump) and the power generated by the PV panels.

$$EER_{grid} = \frac{\dot{Q}_{evap}}{\dot{W}_{grid}} = \frac{\dot{Q}_{evap}}{\dot{W}_{comp} + \dot{W}_{pump} - \sum \dot{W}_{PV}} \tag{28}$$

The results of the optimisation study are presented in Fig. 6. Fig. 6(a) shows the variation of the power consumption and generation as a function of Q. For convenience and better understanding, a dual y-axis chart is used because of the different orders of magnitude observed for the different plotted variables. As expected, $\dot{W}_{comp}$ decreases with Q, from 755.5 to 733.4 W, while $\dot{W}_{pump}$ increases with the flow rate from 26.1 to 187.4 W. The power generated by the 4 panels slightly increases from 736.2 to 762.2 W. Those trends find an optimal value at Q = 1.05 m^3 h^{-1} (Q = 262.5 l h^{-1} each chimney). Although hardly noticeable in this figure, the grid power for this flow rate is 44.3 W. This implies that, under these operating conditions, the system is powered by 44.33 W from the grid. The same conclusion can be reached by observing Fig. 6(b), where the EER and the EER_{grid} are plotted against the water flow rate. Again, each magnitude is presented in a different y-axis (different order of magnitude). A maximum value of EER_{grid} = 85.72 is obtained, matching with the flow rate of minimum power consumption. As explained before, the chiller EER increases until it asymptotically reaches the limit imposed by the condensing temperature, since it only depends on the condenser output water temperature. Finally, the variation of the PV efficiency and module performance parameters with Q is shown in Fig. 6(c). This figure depicts the variation of the module temperature, generated power (one panel) and efficiency against Q. The combined influence of the higher $\dot{m}_a$ (higher water–air momentum exchange) and the lower T_{a_i} (because water temperature reduction) with increasing Q, has a positive effect on η_{PV}. The generated power and the efficiency increase from 184 to 190.5 W and 12.31 to 12.75%, respectively.

3.3. Parametric analysis

As previously stated in Section 1, conducting a parametric analysis aims to independently assess the impact of the ambient conditions on the system's performance, enabling the extrapolation of the performance evaluation to other locations. Four variables were considered in

Table 4
Design ambient and operating conditions considered in the optimisation analysis.

Magnitude	T_{amb} (°C)	ϕ_{amb} (%)	G (W m^{-2})	v_w (m s^{-1})	$\dot{Q}_{evap}$ (kW)	$T_{w_{2_{evap}}}$ (°C)
Value	35.6	35	920.17	3.028	3.8	7

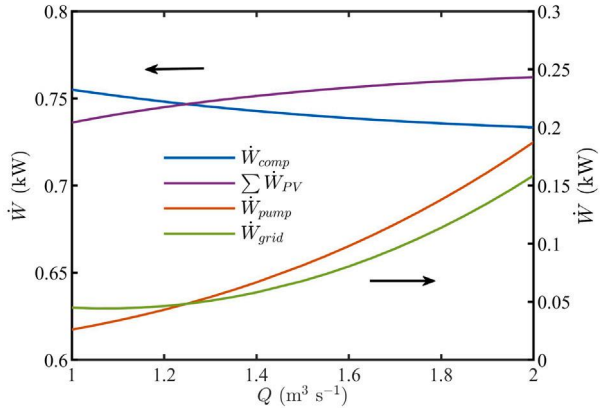

(a) Variation of the power consumption and generation as a function of Q. Left y-axis: $\dot{W}_{\text{comp}}$ and $\sum \dot{W}_{\text{PV}}$. Right y-axis: $\dot{W}_{\text{pump}}$ and $\dot{W}_{\text{grid}}$.

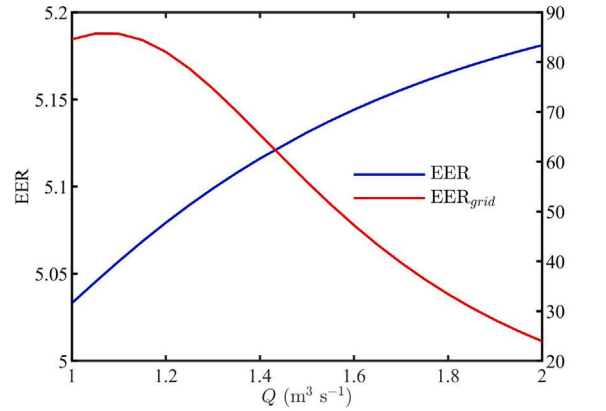

(b) Variation of the EER as a function of Q. Left y-axis: EER. Right y-axis: EER_{grid}.

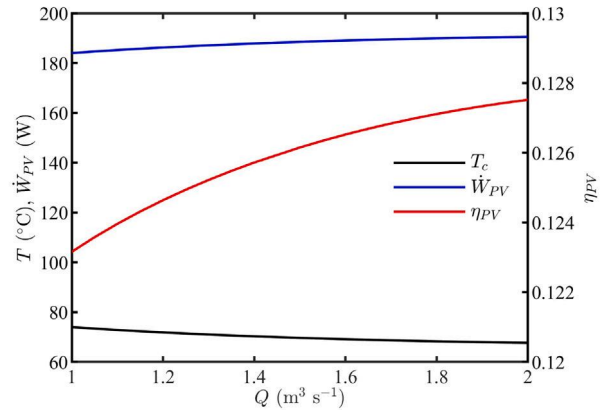

(c) Variation of the PV efficiency and module performance parameters as a function of Q. Left y-axis: $\dot{W}_{\text{PV}}$ and T_c. Right y-axis: η_{PV}. $\dot{W}_{\text{grid}}$.

Fig. 6. Results of the optimisation study.

Table 5
Ambient conditions for the parametric analysis.

T_{amb} (°C)	ϕ_{amb} (%)	G (W m^{-2})	v_w (m s^{-1})
25	25	250	2.5
30	50	500	5
35	75	750	7.5
40	100	1000	10

the parametric study: ambient temperature and relative humidity, solar irradiance and wind velocity. To be studied independently, four levels were taken into account for each variable, for a total of 256 simulations (Table 5). The rest of the inputs were kept constant, with values of $\dot{Q}_{\text{evap}} = 3.8$ kW, $Q = 1.05$ m^3 h^{-1} and $T_{w_{2_{\text{evap}}}} = 7$ °C.

Given the substantial volume of information obtained, this section addresses the impact of the above-mentioned input variables on the main key performance indicators of the system: efficiency of the PV panels and EER of the water-cooled chiller.

Fig. 7 illustrates the variation of η_{PV} with T_{amb} for the different ϕ_{amb}, G and v_w levels analysed. Each subfigure displays the variation of η_{PV} with T_{amb}, and encompasses eight different series representing the four levels of ϕ_{amb} and G investigated. Four subfigures are required to include the different levels of v_w. The ambient conditions, temperature and relative humidity, can have an impact of up to 7.59% on the efficiency of the panels. An increase in the ambient temperature not only worsens the convective heat dissipation in the front side of the panel, but also affects the performance of the evaporative cooling process taking place in the evaporative area of the chimney. This will result in an increase of T_{w_1}, T_{w_2} and also T_{a_i}. Therefore, the heat dissipation in the rear side is also affected via T_{a_i}. Both effects combined result in a higher cell temperature and a lower efficiency. The effect of the ambient relative humidity is similar than the one just described. This magnitude plays an important role in the evaporation process occurring the chimney, increasing T_{w_1} and T_{w_2} and affecting T_{a_i}, T_c and η_{PV}.

The global irradiance also influences the performance of the panels. When radiant power increases, the required heat rate dissipation from the front and rear surfaces of the panel increases as well, even for a constant conversion. This results in a temperature rise in the panel and a decrease in performance. Although differences up 20.01% have been observed in the simulations, it must be taken into account that the level of global irradiance is very similar in different geographic locations with a high cooling demand. This analysis useful when predicting the daily performance of the panels with changes in G.

The wind velocity only affects the convection coefficient in the front side of the panel. The higher the velocity, the more heat can be dissipated and the lower T_c and higher η_{PV}.

The highest efficiency predicted by the simulations is $\eta_{\text{PV}} = 0.1516$ ($T_{\text{amb}} = 25$ °C, $\phi_{\text{amb}} = 25\%$, $G = 250$ W m^{-2} and $v_w = 10$ m s^{-1}) while the lowest is $\eta_{\text{PV}} = 0.1153$ ($T_{\text{amb}} = 40$ °C, $\phi_{\text{amb}} = 100\%$, $G = 1000$ W m^{-2} and $v_w = 2.5$ m s^{-1}), 31.43% difference.

When analysing the influence of the ambient conditions on the EER, it has to be noted that neither G nor v_w affects the energy efficiency ratio of the chiller. The effect of T_{amb} and ϕ_{amb} on the mass transfer processes (evaporation) happening in the evaporative area of the chimney has been previously explained. An increase of any of them will result in a higher pair of water temperatures T_{w_1} and T_{w_2}. As the EER is impacted by the condenser inlet water temperature (T_{w_2}) and the evaporator outlet water temperature, which is kept constant in the simulations, the evolution of T_{w_2} has been included in Fig. 8 to depict

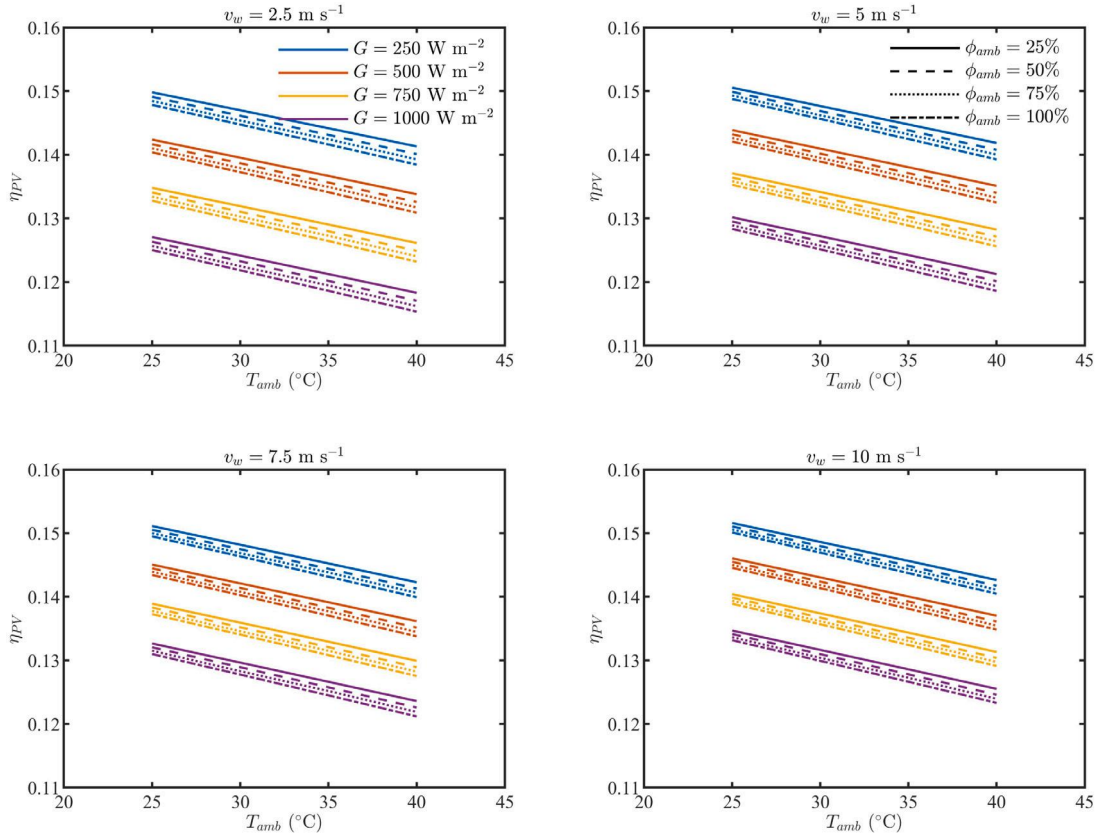

Fig. 7. Variation of η_{PV} with T_{amb} for the different ϕ_{amb}, G and v_w levels analysed. The colours used in the plot refer to different levels of G while various line styles are related to different ϕ_{amb} levels.

the variation the EER with T_{amb} and ϕ_{amb}. As it can be seen, T_{w_2} can increase by 9 °C when increasing T_{amb} for a constant ϕ_{amb} (100%) and surpass 11 °C when increasing ϕ_{amb} for a constant T_{amb} (40 °C). The EER decreases asymptotically with T_{amb} until it reaches a value of EER ∼ 5. The maximum variation for the EER with T_{amb} and ϕ_{amb} is 8.4%.

The findings from this analysis hold significance when extrapolating the system's performance to other locations. For instance, if the system operates in Madrid instead of Alicante, characterised by milder summer temperatures (around 30 °C) and significantly lower humidity levels (around 10% in July), the combined impact of T_{amb} and ϕ_{amb} on PV efficiency can result in differences of up to 5.83%. Regarding heat pump performance, this change in environmental conditions could imply an increase in the EER of 6%. The cumulative enhancements could lead to a 10.86% reduction in energy consumption from the grid while satisfying the same cooling load. These reported differences consider constant irradiance and wind velocity levels.

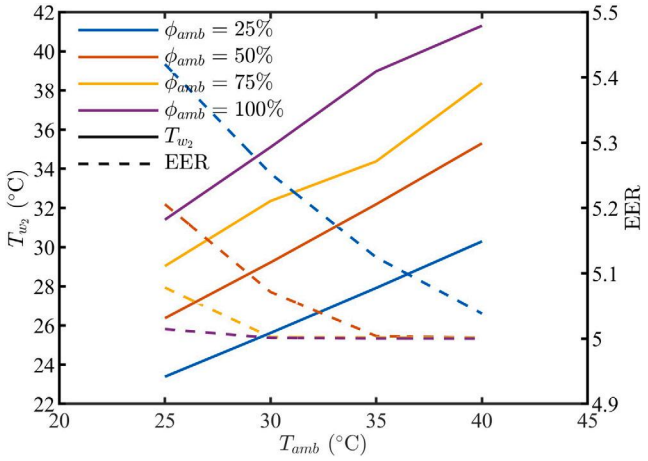

Fig. 8. Variation of T_{w_2} and EER with T_{amb} for the different ϕ_{amb} levels analysed.

3.4. Comparative analysis with other solar cooling technologies

The model of the solar cooling system described in this paper is used to perform a comparative evaluation analysis in this section. In this context, the performance of the system is compared with that of other systems reported in the literature. The research conducted by Aguilar et al. [10] was selected for this purpose. In this study, the authors experimentally analysed the performance of a PV-driven, air–air heat pump used to meet the cooling demand of an office located in Elche (Alicante). The heat pump used in their setup had a nominal cooling capacity of 3.52 kW (very similar to the unit modelled in the present study), and it was driven by three photovoltaic panels with a total peak power of 705 W_p (3×235 W_p). Seventeen different magnitudes were measured every 5 min during 6 months. Two specific days within the experimental campaign were selected for the comparative study: the 18th and 19th of July. These days were chosen not only because the required inputs for the developed model were available but also because, during the 10 am–8 pm period, the heat pump operated at full capacity. Fig. 9 illustrates the evolution of some ambient and operating conditions on these selected days. It includes the cooling load, compressor power consumption, PV generation, power from the grid and solar irradiance. Both were relatively clear days in which the irradiance exceeded 900 W m^{-2} at midday. The cooling load and the compressor consumption remained constant at approximately 3 kW_{th} and 1 kW_e, respectively, during the 10-h period.

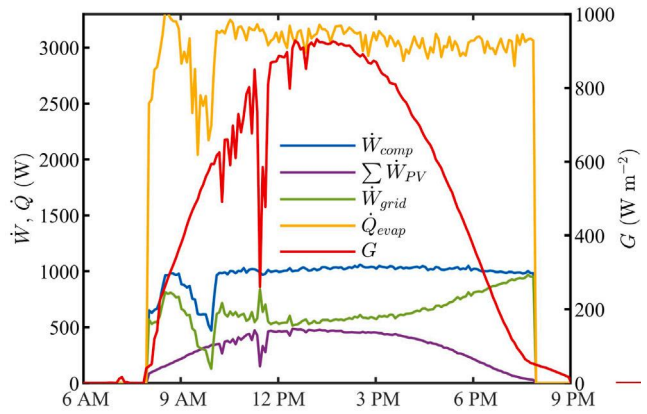

(a) Variation of ambient and operating conditions on the 18^{th} of July.

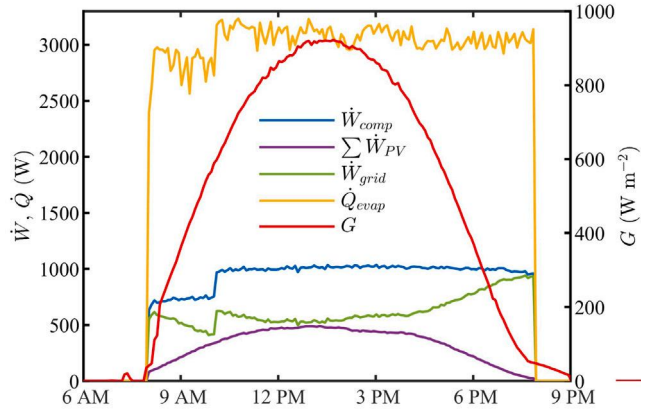

(b) Variation of ambient and operating conditions on the 19^{th} of July.

Fig. 9. Results for two different days included in the experimental campaign reported by Aguilar et al. [10]. The operating conditions are read in the left y-axis while the global irradiance is read in the right y-axis..

Table 6
Daily performance of the solar cooling systems compared.

Magnitude	18th of July		19th of July	
	Experimental	Model	Experimental	Model
Q_{evap} (kWh)	30.47	38	30.49	38
W_{comp} (kWh)	10.04	8.14	9.94	8.12
$W_{comp} + W_{pump}$ (kWh)	10.04	8.47	9.94	8.45
EER (-)	3.03	4.66	3.07	4.67
$\overline{G}$ (kWh m^{-2})	6.426		6.535	
W_{PV} (kWh)	3.77	5.38	3.92	5.01
η_{PV} (%)	11.71	12.98	11.98	12.91

In order to compare the performance of both solar cooling systems, the experimental environmental data (T_{amb}, ϕ_{amb}, G, v_w) collected during the 10-h interval (10 am–8 pm) for the selected days was fed into the model. As in the analyses presented in previous sections, the values for the volumetric flow rate of water, outlet water temperature (cold loop) and heat pump capacity were considered constant and equal to 1.05 m^3 h^{-1}, 7 °C and 3.8 kW, respectively. The results obtained were integrated to derive the energetic performance data, which is presented in Table 6 alongside the experimental results reported for both days.

Although the energy fluxes are not directly comparable because the nominal capacities of the heat pump and the solar field are slightly different, interesting conclusions can be drawn from the key performance indicators of the system: η_{PV} and EER. The proposed system outperforms the solar cooling system outlined in the literature. Regarding the EER of the heat pump, the observed difference is approximately 53% (3 vs. 4.6), indicating a significant reduction in energy consumption (more than half) while delivering an equivalent amount of cooling. As expected, the reduction in the condensing temperature/pressure leads to a decrease in the consumption of the compressor when compared to an air–air heat pump. It is important to note, however, that the reported values correspond to the heat pump's EER, and for a more comprehensive comparison, the pump consumption should be considered in the analysis. The modified EER for the PV evaporative chimney system accounting for the pump consumption, is 4.48 for the 18th of July and 4.49 for the 19th of July, respectively.

Conversely, the PV panels experience enhanced performance with the utilisation of the chimney, with a reported 10% difference when comparing the performances of both systems. It is worth mentioning that the same type of PV panels (polycrystalline) from the same manufacturer was used in both facilities. This increase in the conversion rate is attributed to the cooling effect generated by the air stream induced on the rear side of the panel. Both effects combined, lead to an average grid EER of 12.13 for the 18th of July and 11.04 for the 19th of July, respectively. The obtained values for the EER_{grid} align with the ones outlined by [27], who reported an average of 11.32 cooling kWh per each kWh consumed from the grid. As a final remark, it is emphasised that the performance correlations presented in this paper for the various components (subsystems) of the solar cooling system should be applied for analysing performance within the experimental data collection ranges.

4. Conclusions

In this study, an analytical model of a novel solar cooling system consisting of 4 PV evaporative chimneys and a 3.8 kW water-cooled heat pump has been developed. The model has been validated using experimental data and it has been utilised to analyse the impact of certain environmental variables on the system's performance independently, to optimise the operation to achieve the best energy performance under given environmental and operating conditions, and to compare its energy performance with that of other systems reported in the literature. The results obtained during the investigation can be summarised as follows.

The analytical models of the different components of the system, water-cooled chiller, photovoltaic evaporative chimney and hydraulic hot loop have been linked and the predicted results have been validated with experimental data, showing a maximum average difference for all the variables and test runs compared of 5.83%.

An optimisation analysis based on the grid energy efficiency ratio as key performance indicator has been conducted. It relates the grid electricity required to meet the cooling demand, taking into account the power required to drive compressor and pump and the power generated by the PV panels. The condenser water flow rate was found to be the key variable for the optimisation process. The optimal value for this magnitude was found to be 1.05 m^3 h^{-1} (Q = 262.5 l h^{-1} each chimney). Under this operating conditions, the 3.8-kW cooling load can be met by using only 44.33 W from the grid (EER_{grid} = 85.72).

A comprehensive parametric analysis including the ambient variables was carried out with the aim of independently assessing the impact of the ambient conditions on the system's performance, enabling the extrapolation of the performance evaluation to other locations. The ambient temperature and relative humidity have the greatest influence on the overall system performance. They affect both, the efficiency of the panel via convective heat transfer in the front and rear sides, and the chiller EER via the condenser inlet water temperature. The combined influence of T_{amb} and ϕ_{amb} can lead to differences up to 7.59% in the EER. The highest PV efficiency predicted by the simulations is η_{PV} = 0.1516 and the best EER is 5.42. Under this ambient conditions,

the system is able to convert solar energy into cooling capacity at a rate of 0.822.

Finally, a comparative study considering other solar cooling systems (PV-driven, air–air heat pump) has been conducted. It has been assessed that the use of the solar chimney and the water–water heat pump enhances the overall performance of the system. The predicted values show an improvement of approximately 53% for the chiller EER and 10% for the PV panels conversion efficiency. Both effects combined, lead to an average grid EER of 11.58.

The results obtained during this investigation demonstrate the potential of the proposed solar cooling system to reduce energy consumption in buildings, aligning with Europe's climate commitments. However, certain limitations related to the use of water should be taken into account to assess the technical feasibility of the system. These include, but are not limited to, water consumption, health concerns (legionella), and the need for regular maintenance (nozzle clogging, corrosion, etc.). Future studies should focus on modelling the cooling subsystem, taking into account building usage and ambient conditions, and conducting a comprehensive optimisation analysis to determine the optimal operating conditions based on environmental factors.

CRediT authorship contribution statement

J. Ruiz: Writing – review & editing, Writing – original draft, Validation, Supervision, Methodology, Funding acquisition, Formal analysis. **P. Martínez:** Writing – review & editing, Validation, Methodology. **F. Aguilar:** Writing – review & editing, Methodology, Investigation. **M. Lucas:** Writing – review & editing, Methodology, Formal analysis, Conceptualization.

Declaration of competing interest

The authors declare that they have no known competing financial interests or personal relationships that could have appeared to influence the work reported in this paper.

Data availability

Data will be made available on request.

Acknowledgements

The authors acknowledge the financial support received from the Government of Valencia (Generalitat Valenciana), Spain, through the project GV/2019/008 (Subvenciones para la realización de proyectos de I + D + i desarrollados por grupos de investigación emergentes). The authors also wish to acknowledge the collaboration in the work of the Mechanical Engineering student Francisco José Mallebrera Quesada.

References

[1] D. Mugnier, S.D. White, D. Neyer, The Solar Cooling Design Guide: Case Studies of Successful Solar Air Conditioning Design, Ernst & Sohn, 2017.
[2] D. Neyer, M. Ostheimer, C. Dipasquale, R. Köll, Technical and economic assessment of solar heating and cooling – methodology and examples of iea shc task 53, Sol. Energy 172 (2018) 90–101, Special issue for Solar Cooling.
[3] M.H. Hakemzadeh, K. Sopian, A.F. Abdullah, H. Jarimi, M.F. Fauzan, A. Ibrahim, Technoeconomics of solar thermal-assisted sorption cooling systems under tropical climate condition – a case of malaysia, Energy Convers. Manag.: X 16 (2022) 100305.
[4] P.H. Biwole, P. Eclache, F. Kuznik, Phase-change materials to improve solar panel's performance, Energy Build. 62 (2013) 59–67.
[5] J. Ji, K. Liu, T. tai Chow, G. Pei, W. He, H. He, Performance analysis of a photovoltaic heat pump, Appl. Energy 85 (2008) 680–693.
[6] K. Fong, T. Chow, C. Lee, Z. Lin, L. Chan, Comparative study of different solar cooling systems for buildings in subtropical city, Sol. Energy 84 (2010) 227–244.
[7] T. Otanicar, R.A. Taylor, P.E. Phelan, Prospects for solar cooling – an economic and environmental assessment, Sol. Energy 86 (2012) 1287–1299.
[8] A. Al-Alili, Y. Hwang, R. Radermacher, Review of solar thermal air conditioning technologies, Int. J. Refrig. 39 (2014) 4–22, Solar Cooling.
[9] A. Ghafoor, A. Munir, Worldwide overview of solar thermal cooling technologies, Renew. Sustain. Energy Rev. 43 (2015) 763–774.
[10] F. Aguilar, S. Aledo, P. Quiles, Experimental analysis of an air conditioner powered by photovoltaic energy and supported by the grid, Appl. Therm. Eng. 123 (2017) 486–497.
[11] Z. Song, J. Ji, Z. Li, Comparison analyses of three photovoltaic solar-assisted heat pumps based on different concentrators, Energy Build. 251 (2021) 111348.
[12] A.Y. Sulaiman, G.I. Obasi, R. Chang, H.S. Moghaieb, J.D. Mondol, M. Smyth, B. Kamkari, N.J. Hewitt, A solar powered off-grid air conditioning system with natural refrigerant for residential buildings: A theoretical and experimental evaluation, Clean. Energy Syst. 5 (2023) 100077.
[13] M. Chandrasekar, S. Rajkumar, D. Valavan, A review on the thermal regulation techniques for non integrated flat pv modules mounted on building top, Energy Build. 86 (2015) 692–697.
[14] A. Maleki, A. Haghighi, M. El Haj Assad, I. Mahariq, M. Alhuyi Nazari, A review on the approaches employed for cooling pv cells, Sol. Energy 209 (2020) 170–185.
[15] A. Kaiser, B. Zamora, R. Mazón, J. García, F. Vera, Experimental study of cooling bipv modules by forced convection in the air channel, Appl. Energy 135 (2014) 88–97.
[16] A. Kasaeian, Y. Khanjari, S. Golzari, O. Mahian, S. Wongwises, Effects of forced convection on the performance of a photovoltaic thermal system: An experimental study, Exp. Therm Fluid Sci. 85 (2017) 13–21.
[17] U. Sajjad, M. Amer, H.M. Ali, A. Dahiya, N. Abbas, Cost effective cooling of photovoltaic modules to improve efficiency, Case Stud. Therm. Eng. 14 (2019) 100420.
[18] A.A. Baloch, H.M. Bahaidarah, P. Gandhidasan, F.A. Al-Sulaiman, Experimental and numerical performance analysis of a converging channel heat exchanger for pv cooling, Energy Convers. Manage. 103 (2015) 14–27.
[19] M.S. Ahmed, R. Karal, B.K. Das, A. Das, Experimental investigation of cooling, wind velocity, and dust deposition effects on solar pv performance in a tropical climate in Bangladesh, Case Stud. Therm. Eng. 50 (2023) 103409.
[20] M. Abdolzadeh, M. Ameri, Improving the effectiveness of a photovoltaic water pumping system by spraying water over the front of photovoltaic cells, Renew. Energy 34 (2009) 91–96.
[21] A. Elnozahy, A.K.A. Rahman, A.H.H. Ali, M. Abdel-Salam, S. Ookawara, Performance of a pv module integrated with standalone building in hot arid areas as enhanced by surface cooling and cleaning, Energy Build. 88 (2015) 100–109.
[22] H. Alizadeh, R. Ghasempour, M.B. Shafii, M.H. Ahmadi, W.-M. Yan, M.A. Nazari, Numerical simulation of pv cooling by using single turn pulsating heat pipe, Int. J. Heat Mass Transfer 127 (2018) 203–208.
[23] D.M. Mahmood, I.M.A. Aljubury, Experimental investigation of a hybrid photovoltaic evaporative cooling (pv/ec) system performance under arid conditions, Results Eng. 15 (2022) 100618.
[24] S. Chandel, T. Agarwal, Review of cooling techniques using phase change materials for enhancing efficiency of photovoltaic power systems, Renew. Sustain. Energy Rev. 73 (2017) 1342–1351.
[25] M. Lucas, F. Aguilar, J. Ruiz, C. Cutillas, A. Kaiser, P. Vicente, Photovoltaic evaporative chimney as a new alternative to enhance solar cooling, Renew. Energy 111 (2017) 26–37.
[26] M. Lucas, J. Ruiz, F. Aguilar, C. Cutillas, A. Kaiser, P. Vicente, Experimental study of a modified evaporative photovoltaic chimney including water sliding, Renew. Energy 134 (2019) 161–168.
[27] J. Ruiz, P. Martínez, H. Sadafi, F. Aguilar, P. Vicente, M. Lucas, Experimental characterization of a photovoltaic solar-driven cooling system based on an evaporative chimney, Renew. Energy 161 (2020) 43–54.
[28] P. Casado, J.M. Blanes, F.J.A. Valero, C. Torres, M. Lucas Miralles, J. Ruiz Ramírez, Photovoltaic evaporative chimney i-v measurement system, Energies 14 (2021).
[29] F. Aguilar, On the Influence of Module Temperature on PV Solar Collectors Performance (Master's thesis), Miguel Hernández University, 2008.
[30] E. Skoplaki, J. Palyvos, On the temperature dependence of photovoltaic module electrical performance: A review of efficiency/power correlations, Sol. Energy 83 (2009) 614–624.
[31] R.G. J. Ross, Flat-plate photovoltaic array design optimization, in: 14th Photovoltaic Specialists Conference, pp. 1126–1132.
[32] J. Duffie, W. Beckman, Solar Engineering of Thermal Processes, Wiley, 2013.
[33] V. Sun, A. Asanakham, T. Deethayat, T. Kiatsiriroat, Evaluation of nominal operating cell temperature (noct) of glazed photovoltaic thermal module, Case Stud. Therm. Eng. 28 (2021) 101361.
[34] J. Kloppers, D. Kröger, A critical investigation into the heat and mass transfer analysis of counterflow wet-cooling towers, Int. J. Heat Mass Transfer 48 (2005) 765–777.
[35] F. Merkel, Verdunstungskühlung, VDI Zeitschriff Deutscher Ingenieure, Berlin, Alemania, 1925, pp. 123–128.
[36] M. Poppe, H. Rögener, Berechnung von rückkühlwerken, VDI Wärmeatlas (1991) Mi 1.

[37] P. Navarro, J. Ruiz, M. Hernández, A. Kaiser, M. Lucas, Critical evaluation of the thermal performance analysis of a new cooling tower prototype, Appl. Therm. Eng. 213 (2022) 118719.
[38] G. Bourke, P. Bansal, Energy consumption modeling of air source electric heat pump water heaters, Appl. Therm. Eng. 30 (2010) 1769–1774.
[39] C. Underwood, M. Royapoor, B. Sturm, Parametric modelling of domestic air-source heat pumps, Energy Build. 139 (2017) 578–589.
[40] K.R. Deutz, G.-L. Charles, O. Cauret, R. Rullière, P. Haberschill, Detailed and dynamic variable speed air source heat pump water heater model: Combining a zonal tank model approach with a grey box heat pump model, Int. J. Refrig. 92 (2018) 55–69.
[41] US Department of Energy, Energyplus engineering manual, 2023, Accessed on 2023. https://energyplus.net/documentation.